Effect of Particle Size on the Origin of Electromechanical Response in BaTiO3/PDMS Nanogenerators

Darya Meisak, Artyom Plyushch, Martynas Kinka, Sergejus Balčiunas, Vidmantas Kalendra, Sébastien Schaefer, Aleksej Zarkov, Algirdas Selskis, Juras Banys, Vanessa Fierro, et al.

ACS APPLIED ELECTRONIC MATERIALS

pubs.acs.org/acsaelm

Article

Effect of Particle Size on the Origin of Electromechanical Response in $BaTiO_3$/PDMS Nanogenerators

Darya Meisak,* Artyom Plyushch, Martynas Kinka, Sergejus Balčiūnas, Vidmantas Kalendra, Sébastien Schaefer, Aleksej Zarkov, Algirdas Selskis, Jūras Banys, Vanessa Fierro, and Alain Celzard

Cite This: *ACS Appl. Electron. Mater.* 2024, 6, 7464−7474

Read Online

ACCESS | Metrics & More | Article Recommendations | Supporting Information

ABSTRACT: Polydimethylsiloxane (PDMS)-based composites filled with 80, 300, and 700 nm-sized $BaTiO_3$ (BTO) particles at different concentrations (23, 30, and 40 vol %) were prepared, and their temperature and frequency dielectric properties, as well as electromechanical energy harvesting performance, were studied. BTO/PDMS composites exhibit a low-temperature dynamic glass transition anomaly dependent on BTO size. For 300 and 700 nm-sized tetragonal BTO, the glass transition temperature shifts toward higher temperatures as the filler content increases, due to strong interaction between PDMS and BTO. For 80 nm-sized cubic BTO, a weak interaction between fillers and matrix produces an inverse temperature shift. The electromechanical response in terms of energy harvesting of BTO/PDMS-based nanogenerators, tested under a periodic vertical compression force of 20 N at frequencies of 1−15 Hz, showed an optimal BTO concentration at a certain particle size. The best output parameters were found for 23 vol % of 300 nm-sized BTO, namely, 9.99 V and 2.17 μA for voltage and current, respectively. Two different types of the electromechanical response were detected. Electrostriction and dielectric elastomer capacitor phenomenon are the basic mechanisms by which energy harvesting is explained in pure PDMS and composites with 80 nm-sized BTO. Whereas for the composites with 300 and 700 nm-sized BTO, the piezoelectric effect is responsible for the output performance. This work not only offers a solution for energy harvesting applications but also provides data on dielectric relaxation processes and electromechanical conversion capability as a function of filler size and content.

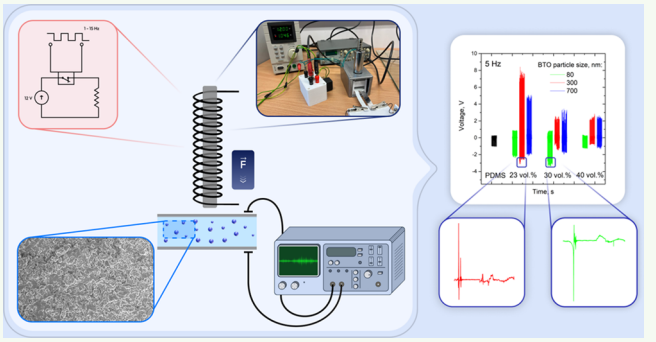

KEYWORDS: *BTO, PDMS, PENG, electromechanical energy harvesting, piezoelectric nanogenerator, dielectric properties, glass transition, particle size, polydimethylsiloxane, barium titanate, composite*

INTRODUCTION

The conversion of low-frequency ambient mechanical energy into electricity, i.e., energy harvesting, is a promising area of research for a broad range of applications, from wearable electronics and self-powered micro/nanosystems[1,2] to bio-implantable applications.[3,4] Devices with such conversion functionality, called electromechanical energy harvesters (or nanogenerators), can operate according to different mechanisms.[5] Specifically, for well-known piezoelectric[6,7] and triboelectric[8] nanogenerators, the operating mechanisms are dipolar induction and contact electrification, respectively. In contrast, the lesser-known ferroelectrets[9] and flexoelectrets[10] operate through pore charging/deformation and strain gradients, respectively. Since the listed modes of operation are not mutually exclusive, they can be combined to improve the nanogenerator's output parameters. For instance, hybrid ferroelectret-piezoelectric,[11] triboelectric-flexoelectric,[12] etc.,[13−17] nanogenerator devices have been reported.

The efficiency of the electromechanical energy harvesting is determined by the deformability of the nanogenerator's active material. Elastic polymers are therefore ideally suited to active materials. Some of them already possess the desired properties (e.g., piezoelectric,[18,19] electrostrictive polymers,[20] etc.) or, alternately, a functional filler can be introduced into the passive polymer matrix.[21,22] A representative of the second group, polydimethylsiloxane (PDMS), as a chemically and thermally stable polymer with remarkable wear resistance and durability, is widely used for nanogenerator design.[14,23−26] Among the many functional fillers for electromechanical nanogenerator design,[27] lead-free perovskite-type tetragonal barium titanate $BaTiO_3$ is especially popular due to its piezoelectric properties. However, its prospects are not limited to piezoelectric nanogenerators:

Received: July 29, 2024
Revised: September 20, 2024
Accepted: September 23, 2024
Published: October 3, 2024

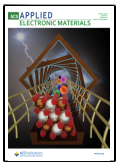

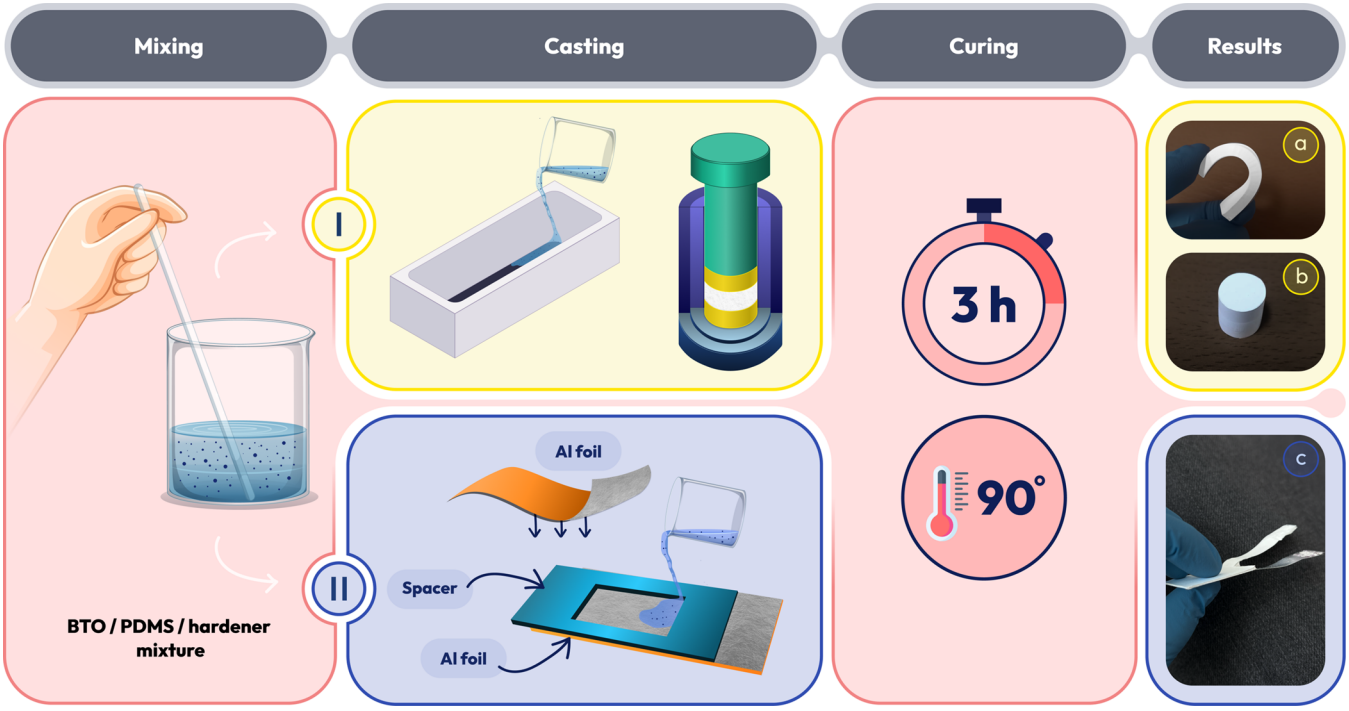

Figure 1. Preparation Procedure for BTO/PDMS composites and nanogenerator devices based on BTO/PDMS composites. Images of (a,b) the prepared composites and (c) the nanogenerator device.

they are also used in harvesters operating based on other mechanisms.[14,23,28,29]

The present article focuses on flexible nanogenerators based on PDMS composites filled with BTO nanoparticles prepared by a simple dispersion method. Regarding composites, the effects of BTO particle size and content on dielectric properties and electromechanical energy harvesting performance are mainly investigated here. Regarding mechanical-to-electrical energy harvesters, while the effects of content are well studied,[14,25,26,28,30] only a few works[23,31] on the effect of particle size can be found. Furthermore, for recording the output parameters of the electromechanical response, a unique experimental setup has been designed and assembled, allowing sample sets to be tested under reproducible conditions (compressive force of 20 N, frequency range of 1−15 Hz). Testing under repeatable mechanical stress conditions offers a clear advantage over finger/foot tapping[24,32,33] or throwing a basketball[34] when it comes to comparing results. The aim of the work was not only to obtain a material suitable for energy harvesting applications but also to understand the characteristics of dielectric relaxation processes, glass transition temperature, and electromechanical response as a function of filler size and content.

MATERIALS AND METHODS

Materials Used. For the preparation of composites, three different commercially available barium titanate ($BaTiO_3$, here referred to as BTO) powders (CAS #12047-27-7) were used. Two types of powder-bearing product numbers US3827 (hereinafter marked as BTO1) and US3829 (BTO2) were received from US Research Nanomaterials, Inc., while the third one, 208108 (BTO3), was provided by Sigma-Aldrich. All the BTO powders mentioned are labeled by their suppliers as tetragonal, and they are supposed to have different particle sizes. Polydimethylsiloxane (PDMS), Sylgard 184 silicone elastomer, was purchased from Dow-Corning (Midland, MI, USA) as a two-part material with a base and curing agent.

Preparation of BTO/PDMS Composites. A simple dispersion method[35] with some modifications based on pressing for the case of high filler content was used to prepare the composites. A set of 9 samples (23, 30, and 40 vol % fractions of each BTO type) was synthesized according to the procedure, whose step-by-step sequence is as follows.

Prior to handling, PDMS was degassed under a vacuum (4000 Pa, 30 min) at room temperature. For each sample, the corresponding amount of BTO particles were dispersed in isopropyl alcohol (IPA) by sonication (ultrasonic bath, VWR USC 1200 TH, 600 W) for 1.5 h. Next, the required amount of degassed uncured PDMS was poured into the BTO/IPA solution, and the resulting mixture was sonicated for 3 additional hours. To evaporate the IPA, the BTO/IPA/PDMS solution was placed overnight in a ventilated oven at 60 °C. For the curing process, a curing agent in a ratio of 1:10 with respect to PDMS was added to the BTO/PDMS mixture, which was then gently stirred manually for 10 min. The following steps are illustrated in Figure 1. More precisely, the resulting slurry, ready to be cast and to undergo final curing, was divided into two parts: the first was used to prepare the composites (Figure 1 - I scheme), while the second was used to manufacture the nanogenerators (Figure 1 - II scheme). Further casting of the first part of the slurry depended on its final viscosity. If the mixture was sufficiently liquid, it was poured into molds and degassed under 4000 Pa until air bubbles were completely eliminated (about 15 min). In contrast, if a paste-like mixture was obtained, it had to be manually pressed. It is important to note here that the viscosity of the final slurry depended not only on the filler concentration but also on the type of BTO powder. For instance, for BTO1 powder, all available concentrations (starting with the lowest one of 23 vol %) had to be pressed, while for both BTO2 and BTO3 powders, only the highest concentration of 40 vol % failed to flow into the mold. Finally, the composites were cured at 90 °C for 3 h. Figure 1a,b shows images of the composites prepared by the two casting methods depending on viscosity.

Fabrication of Nanogenerators Based on BTO/PDMS Composites. The desired final nanogenerator device is a thin BTO/PDMS film of a given geometry placed between two electrodes. To this end (see Figure 1 - II scheme), the second part of the above-mentioned slurry was placed in a 400 μm-thick PTFE-based spacer located

https://doi.org/10.1021/acsaelm.4c01333
ACS Appl. Electron. Mater. 2024, 6, 7464−7474

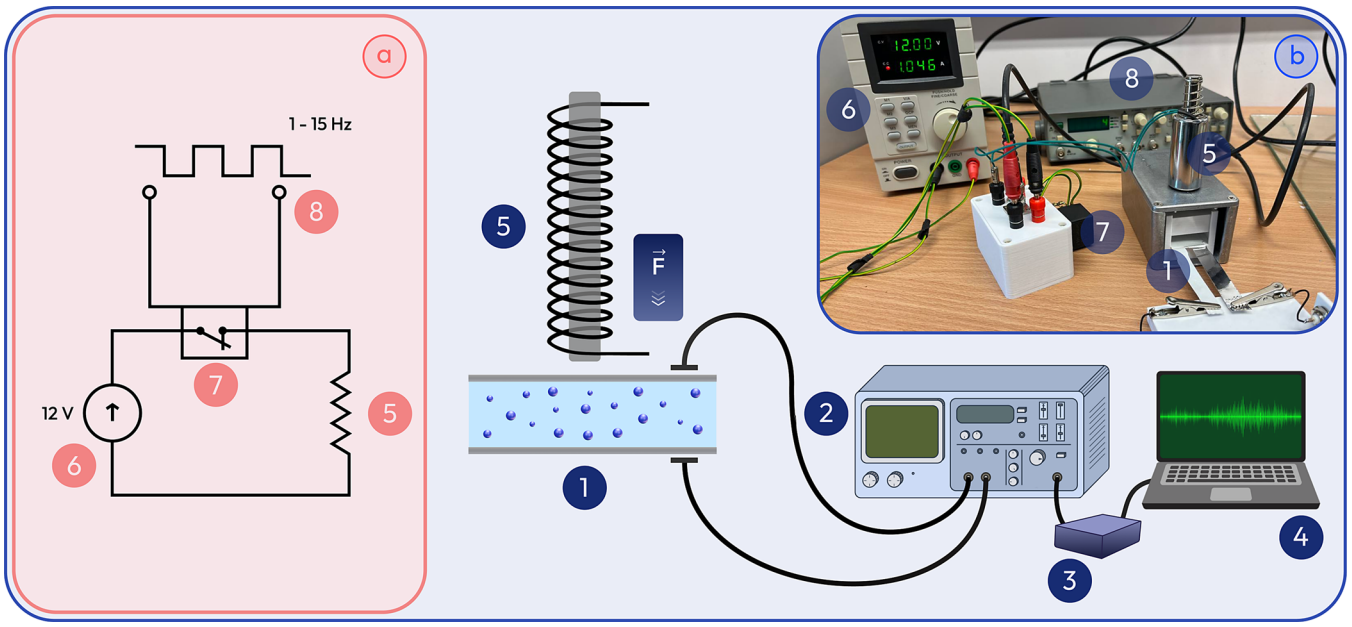

Figure 2. Experimental setup for measuring nanogenerator output characteristics, including (a) electrical diagram of electromagnet powering and (b) photo of its practical implementation: 1 - nanogenerator device (sandwich system of a thin BTO/PDMS composite layer between Al contacts); 2 - oscilloscope; 3 - adapter; 4 - PC; 5 - pushing electromagnet; 6 - DC power supply; 7 - relay; 8 - laboratory generator.

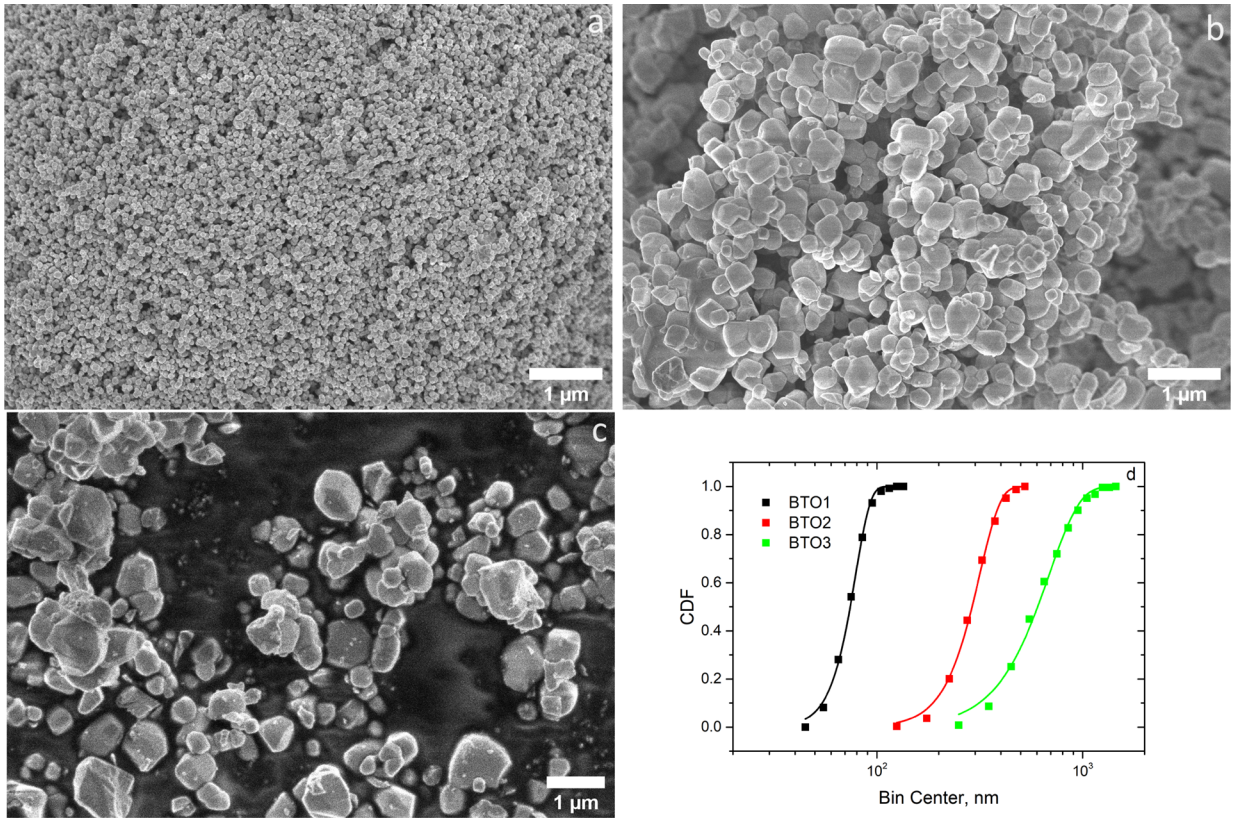

Figure 3. Scanning electron microscopy (SEM) images of (a) BTO1; (b) BTO2; (c) BTO3 powders. (d) Cumulative distribution functions (CDF) for all BTO powders studied.

between two pieces of dense aluminum (Al) foils acting as contacts. This structure was then fixed between two glass plates for the curing process under conditions similar to those for bulk composites (90 °C, 3 h). Once cured, the Al-BTO/PDMS-Al sandwich was carefully cut around the perimeter of the spacer and removed from it. Figure 1c shows a photo of the resulting nanogenerator device. Such structures were prepared for each composition and had the same geometry, controlled by the dimensions of the spacer (2.5 cm × 3 cm surface area, 400 μm thickness). In their present form, the devices are ready for further harvesting measurements and subsequent comparisons of results.

https://doi.org/10.1021/acsaelm.4c01333
ACS Appl. Electron. Mater. 2024, 6, 7464−7474

Characterization Methods. The complex dielectric permittivity of the samples was measured in the 20 Hz to 1 MHz frequency range using an *HP*4284*A* LCR meter. For measurements above room temperature, a laboratory-made furnace was used, while for lower temperatures, a cooling system based on liquid nitrogen was applied. For dielectric tests, plane-parallel samples with a typical thickness of 1 mm and a cross-sectional area of 5 mm^2 with silver paste as the electrical contacts were prepared.

The structure and morphological properties of the samples, as well as the particle size distribution of the powders, were studied by scanning electron microscopy (SEM) using a Helios NanoLab 650 microscope (Thermofisher Scientific, Hillsboro, USA).

X-ray diffraction (XRD) analysis was performed on a Rigaku MiniFlex II diffractometer using Cu Kα radiation (λ = 1.5419 Å) in a Bragg−Brentano ($\theta/2\theta$) geometry. Data were collected over a 2θ angle range of 10°−60° with a speed of 1°/min.

The AixaCCT TF2000 analyzer (Aachen, Germany) equipped with a 4 kV power supply was used for electromechanical property measurements. To apply such high voltage, samples (400 μm-thick) with preapplied silver paste contacts were placed in a chamber filled with mineral oil.

Method for Measuring Nanogenerator Output Performance. The experimental setup for measuring the nanogenerator output characteristics is illustrated schematically in Figure 2. Output performance, including output voltage and current signals, was investigated by applying a repeated vertical compression force ($\vec{F}$) of around 20 N at different frequencies in the 1−15 Hz range. The source of periodic blows was a pushing electromagnet activated when a laboratory generator (ESCORT EGC-3236A) applied via a relay a 12 V periodic pulse signal at the required frequency. The pushing force of the electromagnet was 2 kgf (i.e., a pushing mass of 2 kg with a ground acceleration of 9.8 m/s^2). The electrical diagram of the electromagnet powering is shown schematically in Figure 2a, while Figure 2b shows a photograph of the assembled system. A rectangular tip with an area larger than that of the sample, intended for direct contact with the sample, was prepared using a 3D printer and attached to the moving part of the electromagnet. The output voltage signals appearing on the sample under its external deformation were acquired by a digital oscilloscope (Tektronix TDS 2024B), with the possibility, thanks to a special adapter, of monitoring the results in real-time, as well as exporting and processing the data directly on the PC. A Keithley 6514 electrometer was used for output current measurements.

RESULTS AND DISCUSSION

Characterization of BTO Powders and BTO/PDMS Composites. To estimate the particle size of the BTO powders under study, scanning electron microscopy (SEM) was used for visualization, ImageJ software for statistical data collection, and the Weibull distribution for size magnitude probability modeling.

SEM images of BTO1, BTO2, and BTO3 powders are presented in Figure 3a−c respectively. It is qualitatively obvious that the mean particle size increases from BTO1 to BTO3. To quantify, the cumulative distribution functions (CDFs), obtained from SEM image data and approximated using the expression $1-\exp\left(-(x/\lambda)^m\right)$, for all BTO powders, are presented in Figure 3d. The corresponding parameters are listed in Table 1, where m is the shape parameter (or Weibull modulus), and λ is the scale parameter of the distribution. The third column corresponds to the BTO particle size estimate in the form of a mean value calculation. The values of the mean particle size and parameter λ are consistent. It can therefore be concluded that BTO1, BTO2, and BTO3 powders are characterized by particle sizes of about 80, 300, and 700 nm, respectively. The size of BTO1 powder does not agree with the value claimed by the supplier.

Table 1. Cumulative Distribution Function (CDF) Fitting Parameters for the BTO Powders

powder	m	λ, nm	mean value, nm
BTO1	6.01	78.83	79.15
BTO2	4.30	315.79	316.28
BTO3	2.87	686.47	673.05

Figure 4a−c shows SEM images for 40 vol % BTO/PDMS composites based on all BTO powder types. It is clear that composites with the maximum available filler concentration, regardless of the BTO particle size, are characterized by a fairly homogeneous particle distribution in the PDMS matrix.

X-ray diffraction patterns obtained at room temperature for the 40 vol % BTO/PDMS composites based on all BTO powder types studied are presented in Figure 4d. For the composite with the 80 nm particle size BTO1 powder (red curve), all peaks are identified as the cubic $BaTiO_3$ phase (according to PDF-2 no. 00-075-0212) with space group *Pm*-3*m*. This result contradicts the supplier's claim about the tetragonality of the BTO1 powder provided. In contrast, for 300 nm BTO2 (blue curve) and 700 nm BTO3 (green curve), tetragonal $BaTiO_3$ phases (according to PDF-2 no. 00-081-2201) with space group *P*4*mm* were detected. The ferroelectric state in the 40 vol % BTO2/PDMS and 40 vol % BTO3/PDMS composites is confirmed by a splitting of the peak near 45° into the (002) and (200) planes of $BaTiO_3$.[36] Whereas for the 40 vol % BTO1/PDMS composite, the peak in question is a single, sharp peak revealing the paraelectric order of BTO1.[37] In the XRD patterns of the BTO/PDMS composites of lower concentrations (23 and 30 vol %) and BTO powders, no other structural features were identified (see Supporting Information, Figure S1a,b).

Dielectric Properties. The temperature dependencies of the real (ε') and imaginary (ε'') parts of the complex dielectric permittivity at a frequency of 240 kHz for all of the BTO/PDMS composites studied are presented in Figure 5a,b. Figure 5c shows the temperature dependencies of ε' for the 40 vol % BTO3/PDMS composite at different frequencies. The frequency spectra of ε' at room temperature for all samples and of ε'' at different temperatures for the 40 vol % BTO3/PDMS composite are presented in the Supporting Information (Figure S2a,b).

Over the entire temperature range, the real part of the dielectric permittivity is characterized by an increase in the absolute value with increasing BTO content. Furthermore, at fixed concentrations, depending on the type of BTO powder (particle size), the values of ε' differ within the limits of measurement accuracy and can be considered independent of particle size. Above room temperature and for all composites considered, ε' is characterized by a monotonic decrease upon heating and is independent of frequency (see Figures 5c and S2a). Whereas at low temperatures close to 160 K, a dielectric anomaly associated with relaxation in PDMS is observed (dynamic glass transition). This anomaly consists in the presence of a maximum in the temperature spectra of both the real part of ε and the dielectric losses. The position of these peaks for each particular sample is frequency-dependent and shifts toward higher temperatures with increasing frequency (see Figures 5c and 6a). The dielectric anomaly discussed is also reflected in the frequency spectra, namely, that a maximum of the imaginary part of the dielectric permittivity is observed. Moreover, the frequency at the ε'' maximum decreases with cooling (see Figure S2b).

https://doi.org/10.1021/acsaelm.4c01333
ACS Appl. Electron. Mater. 2024, 6, 7464−7474

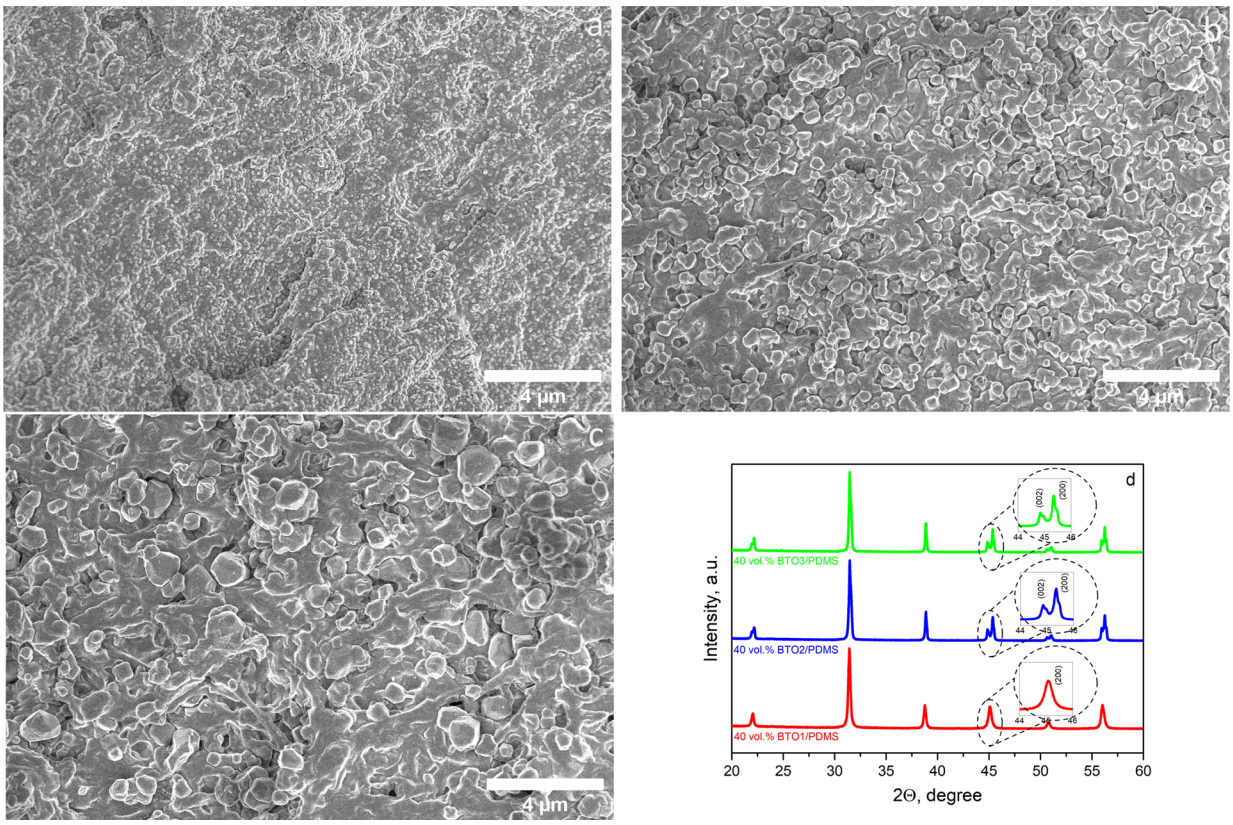

Figure 4. Scanning electron microscopy (SEM) images of 40 vol % (a) BTO1/PDMS; (b) BTO2/PDMS; and (c) BTO3/PDMS composites. (d) XRD patterns for 40 vol % BTO/PDMS composites based on all BTO powder types studied.

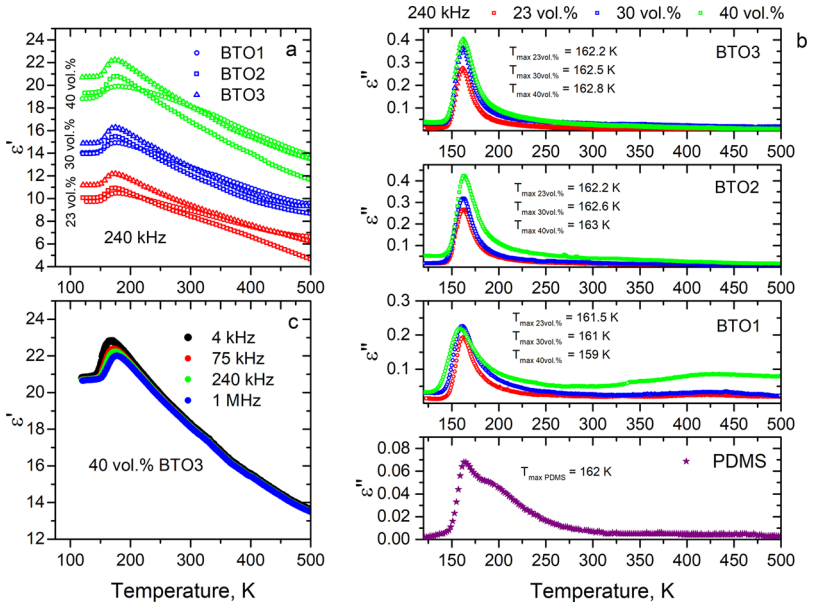

Figure 5. Temperature dependencies of (a) the real and (b) the imaginary parts of the dielectric permittivity at 240 kHz frequency for 23, 30, and 40 vol % BTO/PDMS composites and pure PDMS. (c) Temperature dependencies of the real part of the dielectric permittivity at different frequencies for the 40 vol % BTO3/PDMS composite.

The dielectric losses maximum and its shift relative to pure PDMS as a function of filler concentration depend on BTO particle size (see Figure 5b). For BTO2 (300 nm) and BTO3 (700 nm) powders, as the filler concentration increases, the ε'' peak shifts to the higher temperatures region (to the right of pure PDMS), while for the powder with the smallest particle size of 80 nm (BTO1), the shift occurs to the lower temperatures region (to the left of pure PDMS).

The frequency dependence of the position of the dielectric losses maximum (see Figure 6a) for all the composites studied obeys the Vogel–Fulcher law (see Figure 6c):

https://doi.org/10.1021/acsaelm.4c01333
ACS Appl. Electron. Mater. 2024, 6, 7464−7474

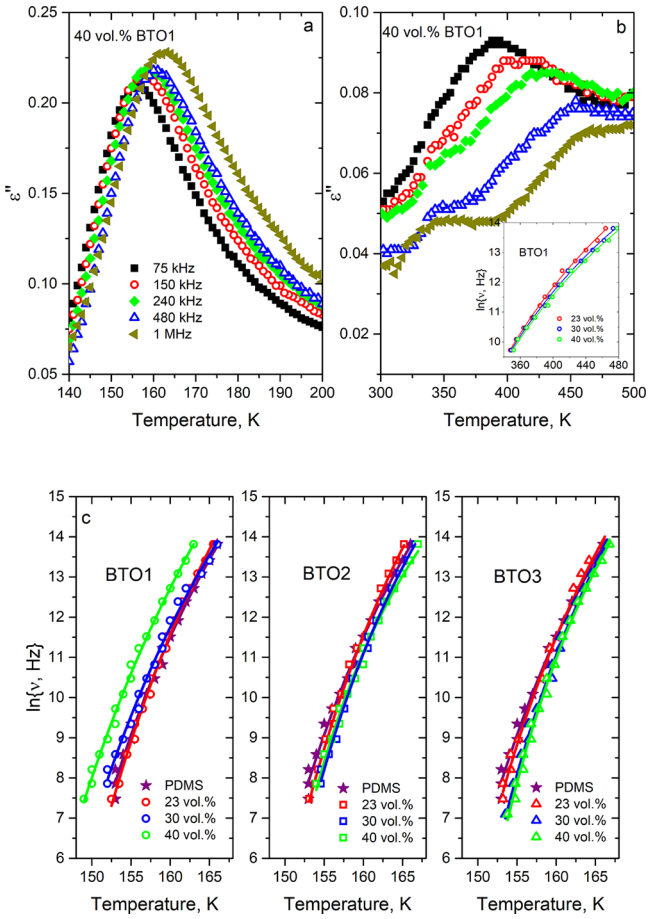

Figure 6. Temperature dependencies of dielectric losses at different frequencies for 40 vol % BTO1/PDMS composite (a) below and (b) above room temperature. Inset: Frequency versus temperature at maximum dielectric losses for BTO1/PDMS composites (at high temperatures). Solid lines are best fits to the Arrhenius model, eq 2. (c) Frequency versus temperature at maximum dielectric losses for BTO/PDMS composites at 23, 30, and 40 vol % and pure PDMS (at low temperatures). Solid lines are best fits to Vogel–Fulcher eq 1.

$$\nu = \nu_0 \exp \frac{-E_{VF}}{k_B(T_{max} - T_{ref})} \quad (1)$$

where T_{ref} is the glass transition temperature of the polymer, T_{max} is the temperature at the dielectric loss maximum, k_B is the Boltzmann constant, ν_0 is the frequency at very high T_{max}, and E_{VF} is the Vogel–Fulcher activation energy.

The best Vogel–Fulcher fit parameters to the experimental data for all of the BTO/PDMS composites studied and pure PDMS are listed in Table 2. There is an obvious correlation between the fitting parameters obtained (Table 2) and the pattern of dielectric loss peak shift behavior (Figure 5b). Specifically, for BTO2 and BTO3, the glass transition temperature increases with filler concentration (activation energy E_{VF} decreases), while for BTO1, T_{ref} decreases (E_{VF} increases).

Two cases are possible depending on the impact of particle addition on the mobility of polymer molecules, which directly determines the character of the glass transition process in the polymer. The first case of T_{ref} increase is associated with a reduction in the mobility of the polymer chains due to their strong interaction with the introduced filler particles.[38,39] On the other hand, the decrease in glass transition temperature can be explained by the decrease in polymer density due to the weak interaction between particles and polymer chains.[40,41]

Table 2. Glass Transition Temperatures and Vogel–Fulcher and Arrhenius Activation Energies of BTO/PDMS Composites

sample	ν_0, THz	E_{VF}/k_B, K	T_{ref}, K	ν_{00}, THz	E_A/k_B, K
pure PDMS	9.29	782.37	117.38		
BTO1					
23 vol.%	127.61	926.69	115.69	0.17	5600.20
30 vol.%	32.10	946.01	111.12	0.07	5340.85
40 vol.%	734.34	1195.56	104.40	0.05	5252.23
BTO2					
23 vol.%	27.08	765.66	120.54		
30 vol.%	1.28	571.52	125.96		
40 vol.%	0.03	366.50	131.46		
BTO3					
23 vol.%	7.68	706.66	121.11		
30 vol.%	5.81	657.98	124.11		
40 vol.%	0.37	475.73	129.64		

Returning to the composite system under consideration, dielectric spectroscopy has shown that glass transition in BTO/PDMS composites depends on the BTO particle size. Namely, larger particles 300 (BTO2) and 700 (BTO3) nm in size actively interact with PDMS polymer chains, while smaller particles of BTO1 (80 nm) powder have a weak interaction or are even repelled by polymer molecules. This behavior is due to an increase in the specific surface area of the particles as their size decreases.[42] The latter observation clarifies the difficulties of dispersing BTO1 powder in PDMS during the sample preparation process when even the smallest present concentration of 23 vol % had to be pressed due to its high viscosity.

In summary, the properties of BTO/PDMS composites can be adjusted by selecting the BTO particle size and controlling the BTO concentration. In particular, increasing the BTO concentration monotonically shifts the glass transition temperature of the polymer, and the BTO particle size determines the direction of this shift relative to pure PDMS. This is an interesting result for materials science in the field of functional materials.

Moreover, at higher temperatures for BTO1/PDMS composites, a second anomaly of dielectric losses is observed (Figure 5b). The higher the BTO1 concentration, the higher the temperature of the ε'' maximum at a fixed frequency. Since this peak was not observed for pure PDMS, its presence is determined by the filler and related to polarization at the interfacial boundaries (so-called Maxwell–Wagner relaxation). The position of the ε'' peak was also found to be frequency-dependent (see Figure 6b), obeying Arrhenius's law (see Figure 6b inset):

$$\nu = \nu_{00} \exp \frac{-E_A}{k_B T_{max}} \quad (2)$$

where E_A is the Arrhenius activation energy.

The fitting parameters E_A for the BTO1/PDMS composites are shown in Table 2. The activation energies decrease with increasing BTO1 concentration, indicating a significant effect of the addition of BTO1 particles on the properties of BTO1/PDMS composites. The Maxwell–Wagner relaxation frequency is supposed to shift to lower frequencies as particle size increases. Thus, for BTO2/PDMS and BTO3/PDMS composites, a high-

https://doi.org/10.1021/acsaelm.4c01333
ACS Appl. Electron. Mater. 2024, 6, 7464–7474

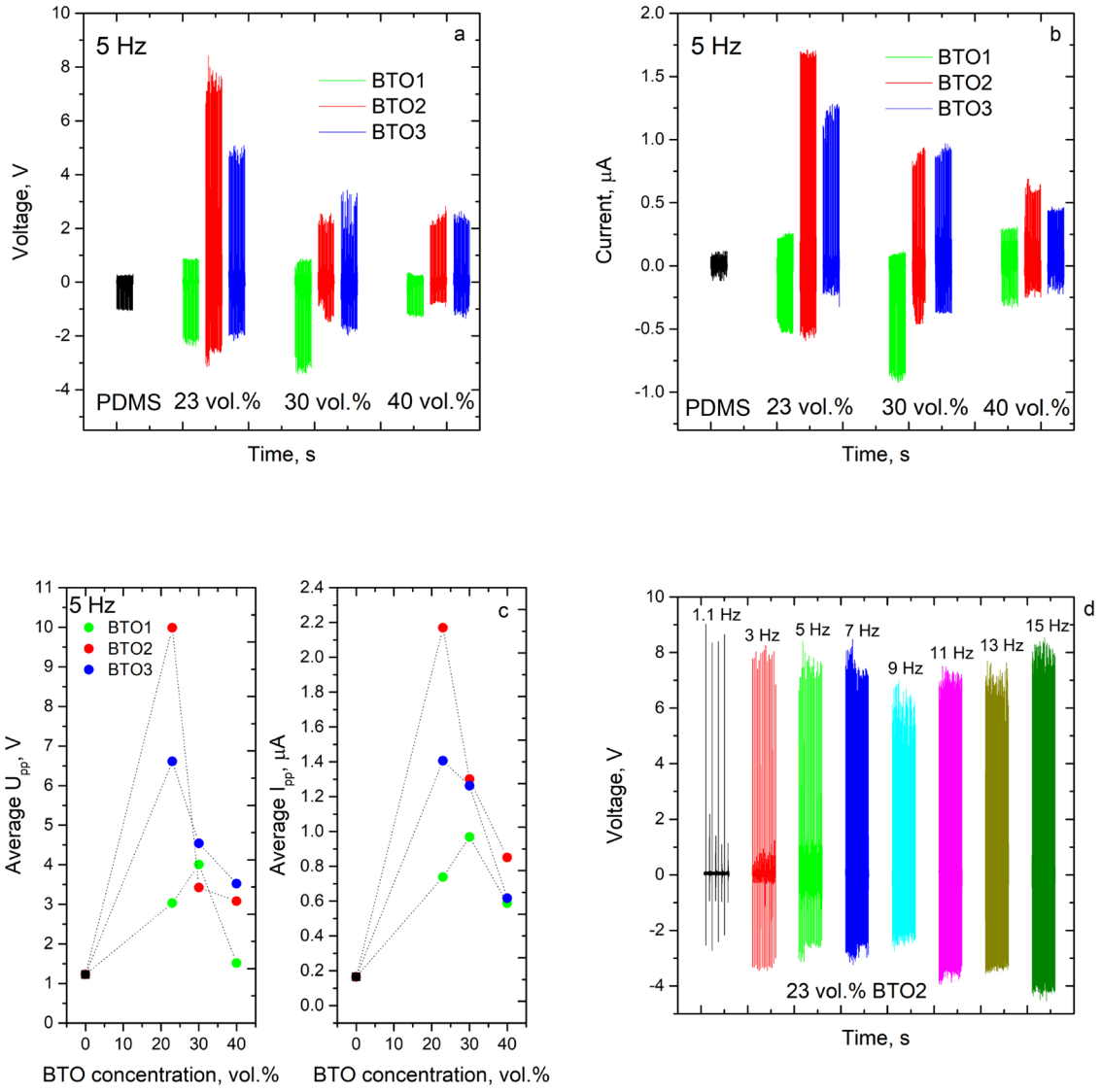

Figure 7. Output (a) voltage and (b) current signals generated by nanogenerator devices based on 23, 30, and 40 vol % BTO/PDMS composites and pure PDMS under a periodic compressive force of 20 N at a frequency of 5 Hz. (c) BTO concentration dependencies of average peak-to-peak output voltages and currents at 5 Hz. (d) Output voltage signals generated by the 23 vol % BTO2/PDMS sample at different frequencies in the 1−15 Hz range.

temperature anomaly was not detected, as it lies outside the range studied.

Energy Harvesting Output Performance. Energy harvesting output characteristics were measured for all 400 μm-thick nanogenerators based on BTO/PDMS composites studied under a periodic compressive force of 20 N at a frequency of 5 Hz. The results of the output voltage and current signals are presented in Figure 7a,b, respectively. Besides, the average peak-to-peak (of total amplitude) voltage U_{pp} and current I_{pp} are plotted as a function of the BTO volume ratio in Figure 7c.

Voltage and current signals from BTO/PDMS nanogenerators show the same trend. First, pure PDMS exhibits a nonzero signal (1.23 V and 0.17 μA), which increases with the addition of BTO, irrespective of filler content and particle size. This increase in signal as a function of content is nonlinear and is characterized by the presence of a maximum, i.e. an optimum concentration. The position of the maximum (see Figure 7c) differs according to the type of BTO powder: for BTO1 powder, the maximum is observed at 30 vol %, while for BTO2 and BTO3, it is at 23 vol. %. At higher concentrations (30 and 40 vol %), the signal level becomes weakly dependent on BTO particle size, while for 23 vol % BTO/PDMS samples, the peak signals show a strong dispersion (from 3 to 10 V for voltage and from 0.7 to 2.2 μA for current). Moreover, at this 23 vol.% concentration, the particle size dependencies also demonstrate a maximum at 300 nm. The phenomenon of optimum concentration was to be expected since it has been observed repeatedly in similar works,[14,23,43] attributed to the impact of filler agglomeration at high concentrations.

The best output signals were observed for the 23 vol % BTO2 (300 nm) nanogenerator and amounted to 9.99 V and 2.17 μA for voltage and current, respectively. For this sample, output characteristics were investigated as a function of frequency in the 1−15 Hz range; results for voltage are presented in Figure 7d, while results for current can be seen in the Supporting Information (Figure S3). According to the results, output performance is almost independent of the frequency in the range considered.

https://doi.org/10.1021/acsaelm.4c01333
ACS Appl. Electron. Mater. 2024, 6, 7464−7474

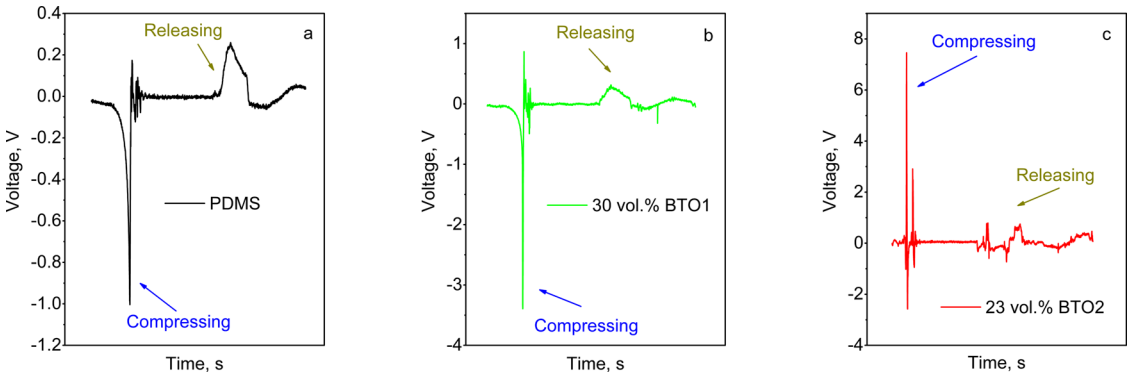

Figure 8. Examples of output voltage signal profiles corresponding to one 20 N-blow at 5 Hz: (a) pure PDMS, (b) 30 vol % BTO1/PDMS, and (c) 23 vol % BTO2/PDMS composites.

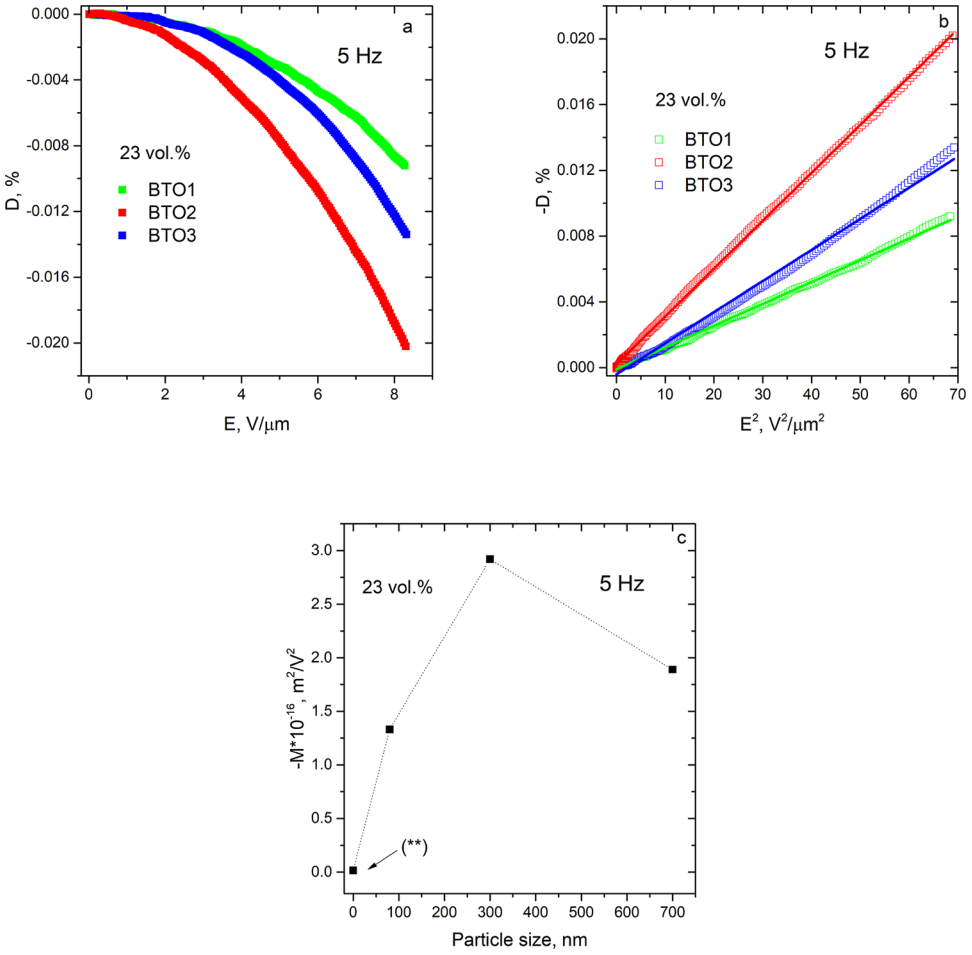

Figure 9. Curves of (a) deformation versus E and (b) strain versus E^2, as well as (c) particle size dependence of the apparent electrostrictive coefficient M for 23 vol.% BTO/PDMS composites at 5 Hz (**M data for pure PDMS were taken from ref 44).

Several physical mechanisms are responsible for converting mechanical stress into electricity. Mainly, all materials exhibit electrostriction. In particular, the electrostrictive coefficient of pure PDMS is around $M = -1.5 * 10^{-18}$ m^2/V^2.[44] The polymer layer with applied electrodes formed a capacitor. Compression of the electrodes increased the electrical capacity of the system. At the release step, the capacitor returns to its initial form and, according to the principle of dielectric elastomers,[45] provides an increase in voltage. The combination of these two mechanisms describes the electromechanical response of pure PDMS. Indeed, as shown in Figure 8a, when a force of 20 N is applied, the voltage decreases along an exponential curve, followed by a series of short positive and negative peaks. These peaks are attributed to the excitation of membrane-type oscillations in the composite.[46,47] The release step causes the voltage across the capacitor electrodes to rise, followed by a relatively slow discharge. The profiles of the output current signals exhibit the same trend as the voltage, and they can be seen in the Supporting Information (Figure S4).

The addition of BTO is expected to have a number of effects. Namely, inhomogeneity boosts electrostriction due to the creation of new interfaces[48] (see Figure 9). Besides, the presence

https://doi.org/10.1021/acsaelm.4c01333
ACS Appl. Electron. Mater. 2024, 6, 7464−7474

of BTO increases capacitance (Figure 5a), leading to an amplification of the dielectric elastomer effect. Stiffening of the system at higher concentrations is the negative effect that suppresses mechanical deformation, resulting in the suppression of the electromechanical response for all samples studied.

The incorporation of cubic BTO1 increases the response compared with that of PDMS (see Figure 8b). The shape of the signal after application and release of force is the same as that of pure PDMS. This suggests that the underlying physics of these systems is similar. Samples containing tetragonal BTO2 and BTO3 show different shape responses (Figures 8c and S5 in the Supporting Information). Short positive peaks are detected on application and release. This is probably due to the piezoelectric term.

Electromechanical properties (i.e., mechanical deformation D versus electric field E) were measured for 23 vol % BTO/PDMS composites at the frequency of 5 Hz at room temperature (see Figure 9a). The parabolic deformation response observed as a function of E (electrostrictive-type shape) has a negative sign that corresponds to compression, which is generally typical for polymers.[49] The strain amplitude reaches a maximum at 300 nm (BTO2) and then at 700 nm (BTO3) decreases but is not lower than at 80 nm (BTO1).

Linear curves, obtained by plotting $-D$ versus E^2 (see Figure 9b), give the apparent electrostrictive coefficient M, linked to the slope of the curves. The "apparent" coefficient includes two components: normal electrostriction and dielectric elastomer's capacitor effects.[48] M values are presented as a function of particle size for 23 vol % BTO/PDMS composites at 5 Hz, as shown in Figure 9c. First, after the addition of 23 vol.% BTO (any size) to PDMS, the apparent value of the electrostriction coefficient increases by 2 orders of magnitude compared with pure PDMS.[44] Second, $-M$ exhibits the same trend (maximum at 300 nm) as the amplitude of the deformation (Figure 9a) and the output voltage and current signals (Figure 7a–c).

Additionally, it is important to note that the 10^{-16} order of magnitude of the electrostriction coefficient is considered high.[44,50] Therefore, electrostriction can be defined as a dominant energy harvesting mechanism, although clearly not the only one, for all of the BTO/PDMS (and pure PDMS) composites studied, without exception.

The piezoelectric impact of BTO2 and BTO3 was difficult to detect in direct D–E measurements, as the strong negative electrostriction suppresses the positive piezoelectric term. However, upon harvesting, due to the deformations of the nanogenerator, and consequently mechanical strength of the BTO particle, the sharp positive peaks in Figure 8c appear for both the application and release steps. For larger particles (700 nm in size), the piezoelectric impact should be higher, since the piezoelectric coefficient increases with particle size[51] However, per unit volume, the number of smaller particles is greater, which determines the maximum overall output response at 300 nm.

CONCLUSIONS

A simple dispersion method was successfully applied to prepare a system of composites based on BTO nanoparticles of three different sizes (80, 300, and 700 nm) at various concentrations (23, 30, and 40 vol %) in a PDMS matrix. Each formulation was cast in two forms: as bulk BTO/PDMS composites for dielectric measurements as well as Al-BTO/PDMS-Al sandwich nanogenerator devices for measurements of energy harvesting parameters. Regarding the dielectric properties of BTO/PDMS composites, the absolute value of the dielectric permittivity increases with the concentration of BTO of a certain particle size, while it is practically independent of particle size at a fixed concentration. Besides, at low temperatures, all composites exhibit a dynamic glass transition anomaly in PDMS, whose behavior depends on the BTO particle size. Specifically, for larger tetragonal particles of 300 and 700 nm in size, the Vogel–Fulcher glass transition temperature shifts to higher temperatures from 120.54 to 131.46 K and from 121.11 to 129.64 K, respectively, due to the strong interaction between PDMS chains and BTO nanoparticles. For smaller cubic particles of 80 nm in size, the glass transition temperature shifts to lower temperatures, from 115.69 to 104.40 K, due to the weak interaction between nanoparticles and polymer chains. Moreover, at higher temperatures of around 400 K, the Maxwell–Wagner relaxation process is detected for composites with 80 nm-sized particles. In addition, nanogenerator devices based on the BTO/PDMS composite have been studied for their response to energy harvesting under a periodic vertical compressive force of 20 N in a frequency range of 1–15 Hz. To this end, a unique experimental setup was designed and assembled, allowing us to perform tests under identical conditions from sample to sample. The concentration dependencies of the output voltage and current signals are characterized by the presence of a maximum, i.e., an optimum BTO volume fraction for which the output parameters reach their highest value for one given size of BTO particle. The best result for output characteristics was achieved for the sample containing 23 vol.% of 300 nm-sized BTO, i.e., 9.99 V and 2.17 μA for voltage and current, respectively. Electrostriction and the phenomenon of a dielectric elastomer capacitor are the dominant mechanisms responsible for mechanical-to-electrical conversion for all BTO/PDMS composites (including pure PDMS) studied. This is confirmed by the estimation of the apparent electrostrictive coefficient, which exhibits the same trend as that of the output voltage and current signals. The presence of a piezoelectric contribution to energy harvesting for samples with tetragonal BTO particles (300 and 700 nm-sized) was observed for concentrations of 23 and 30 vol %, as shown by differences in the shape of the signal profile. The result of this work is therefore not only a material suitable for energy harvesting applications but also systematic data on dielectric relaxation processes and electromechanical output performance as a function of filler size and content.

ASSOCIATED CONTENT

Supporting Information

The Supporting Information is available free of charge at https://pubs.acs.org/doi/10.1021/acsaelm.4c01333.

XRD patterns of BTO/PDMS composites and BTO powders; frequency spectra of the dielectric permittivity; output current signals from the 23 vol.% BTO2/PDMS composite at frequencies from 1 to 10 Hz; profiles of output current signals for BTO/PDMS composites; and profiles of output voltage signals for BTO/PDMS composites (PDF)

AUTHOR INFORMATION

Corresponding Author

Darya Meisak − *Faculty of Chemistry and Geosciences, Vilnius University, 03225 Vilnius, Lithuania; Faculty of Physics, Vilnius University, 10222 Vilnius, Lithuania;* orcid.org/0000-0002-6249-2181; Email: darya.meisak@ff.vu.lt

https://doi.org/10.1021/acsaelm.4c01333
ACS Appl. Electron. Mater. 2024, 6, 7464–7474

Authors

Artyom Plyushch − *Faculty of Physics, Vilnius University, 10222 Vilnius, Lithuania*

Martynas Kinka − *Faculty of Physics, Vilnius University, 10222 Vilnius, Lithuania*

Sergejus Balčiūnas − *Faculty of Physics, Vilnius University, 10222 Vilnius, Lithuania*

Vidmantas Kalendra − *Faculty of Physics, Vilnius University, 10222 Vilnius, Lithuania*

Sébastien Schaefer − *ICMN, UMR 7374, Université d'Orléans-CNRS, 45071 Orléans, France;* orcid.org/0000-0002-6299-0340

Aleksej Zarkov − *Faculty of Chemistry and Geosciences, Vilnius University, 03225 Vilnius, Lithuania;* orcid.org/0000-0002-3574-2296

Algirdas Selskis − *Center for Physical Science and Technology, 10257 Vilnius, Lithuania*

Jūras Banys − *Faculty of Physics, Vilnius University, 10222 Vilnius, Lithuania*

Vanessa Fierro − *CNRS, IJL, Université de Lorraine, 88051 Epinal, France;* orcid.org/0000-0001-7081-3697

Alain Celzard − *CNRS, IJL, Université de Lorraine, 88051 Epinal, France; Institut Universitaire de France (IUF), 75231 Paris, France;* orcid.org/0000-0003-0073-9545

Complete contact information is available at: https://pubs.acs.org/10.1021/acsaelm.4c01333

Notes

The authors declare no competing financial interest.

■ ACKNOWLEDGMENTS

D.M. gratefully acknowledges funding from the Research Council of Lithuania (LMTLT), under agreement no S-PD-22-90. The authors thank Victoria Kravchenko and Uladzislau Pirtan for valuable discussions.

■ REFERENCES

(1) Wang, Z. L.; Wu, W. Nanotechnology-enabled energy harvesting for self-powered micro-/nanosystems. *Angew. Chem., Int. Ed.* **2012**, *51*, 11700−11721.

(2) Wang, B.; Zhong, J.; Zhong, Q.; Wu, N.; Cheng, X.; Li, W.; Liu, K.; Huang, L.; Hu, B.; Zhou, J. Sandwiched composite fluorocarbon film for flexible electret generator. *Adv. Electron. Mater.* **2016**, *2*, No. 1500408.

(3) Dagdeviren, C.; Yang, B. D.; Su, Y.; Tran, P. L.; Joe, P.; Anderson, E.; Xia, J.; Doraiswamy, V.; Dehdashti, B.; Feng, X.; et al. Conformal piezoelectric energy harvesting and storage from motions of the heart, lung, and diaphragm. *Proc. Natl. Acad. Sci. U. S. A.* **2014**, *111*, 1927−1932.

(4) Kim, D.-H.; Viventi, J.; Amsden, J. J.; Xiao, J.; Vigeland, L.; Kim, Y.-S.; Blanco, J. A.; Panilaitis, B.; Frechette, E. S.; Contreras, D.; et al. Dissolvable films of silk fibroin for ultrathin conformal bio-integrated electronics. *Nature materials* **2010**, *9*, 511−517.

(5) Sherrell, P. C.; Šutka, A.; Timusk, M.; Šutka, A. Alternatives to Fluoropolymers for Motion-Based Energy Harvesting: Perspectives on Piezoelectricity, Triboelectricity, Ferroelectrets, and Flexoelectricity. *Small* **2024**, *20*, No. 2311570.

(6) Briscoe, J.; Dunn, S. Piezoelectric nanogenerators−a review of nanostructured piezoelectric energy harvesters. *Nano Energy* **2015**, *14*, 15−29.

(7) Jeong, C. K.; Lee, J. H.; Hyeon, D. Y.; Kim, Y.-G.; Kim, S.; Baek, C.; Lee, G.-J.; Lee, M.-K.; Park, J.-J.; Park, K.-I. Piezoelectric energy conversion by lead-free perovskite BaTiO3 nanotube arrays fabricated using electrochemical anodization. *Appl. Surf. Sci.* **2020**, *512*, No. 144784.

(8) Wang, Z. L. Triboelectric nanogenerators as new energy technology and self-powered sensors−Principles, problems and perspectives. *Faraday Discuss.* **2014**, *176*, 447−458.

(9) Li, W.; Torres, D.; Wang, T.; Wang, C.; Sepúlveda, N. Flexible and biocompatible polypropylene ferroelectret nanogenerator (FENG): On the path toward wearable devices powered by human motion. *Nano energy* **2016**, *30*, 649−657.

(10) Huang, S.; Qi, L.; Huang, W.; Shu, L.; Zhou, S.; Jiang, X. Flexoelectricity in dielectrics: Materials, structures and characterizations. *J. Adv. Dielectr.* **2018**, *8*, 1830002.

(11) Song, Y.; Wu, T.; Bao, J.; Xu, M.; Yang, Q.; Zhu, L.; Shi, Z.; Hu, G.-H.; Xiong, C. Porous cellulose composite aerogel films with super piezoelectric properties for energy harvesting. *Carbohydr. Polym.* **2022**, *288*, No. 119407.

(12) Kim, S. Y.; Jang, S.; Kim, K. N.; Lee, S.; Chang, H.; Yim, S.; Song, W.; Lee, S.; Lim, J.; Myung, S. Multilayered MoS2 Sphere-Based Triboelectric−Flexoelectric Nanogenerators as Self-Powered Mechanical Sensors for Human Motion Detection. *ACS Applied Nano Materials* **2022**, *5*, 15192−15200.

(13) Qi, Y.; Jafferis, N. T.; Lyons, K., Jr; Lee, C. M.; Ahmad, H.; McAlpine, M. C. Piezoelectric ribbons printed onto rubber for flexible energy conversion. *Nano Lett.* **2010**, *10*, 524−528.

(14) Suo, G.; Yu, Y.; Zhang, Z.; Wang, S.; Zhao, P.; Li, J.; Wang, X. Piezoelectric and triboelectric dual effects in mechanical-energy harvesting using BaTiO3/polydimethylsiloxane composite film. *ACS Appl. Mater. Interfaces* **2016**, *8*, 34335−34341.

(15) Chun, J.; Kim, J. W.; Jung, W.-s.; Kang, C.-Y.; Kim, S.-W.; Wang, Z. L.; Baik, J. M. Mesoporous pores impregnated with Au nanoparticles as effective dielectrics for enhancing triboelectric nanogenerator performance in harsh environments. *Energy Environ. Sci.* **2015**, *8*, 3006−3012.

(16) Yan, D.; Wang, J.; Xiang, J.; Xing, Y.; Shao, L.-H. A flexoelectricity-enabled ultrahigh piezoelectric effect of a polymeric composite foam as a strain-gradient electric generator. *Sci. Adv.* **2023**, *9*, No. eadc8845.

(17) Kim, Y.-g.; Kim, H.; Lee, G.-J.; Lee, H.-U.; Lee, S. G.; Baek, C.; Lee, M.-K.; Park, J.-J.; Wang, Q.; Cho, S. B.; et al. Flexoelectric-boosted piezoelectricity of BaTiO3@ SrTiO3 core-shell nanostructure determined by multiscale simulations for flexible energy harvesters. *Nano Energy* **2021**, *89*, No. 106469.

(18) Broadhurst, M.; Davis, G. Physical basis for piezoelectricity in PVDF. *Ferroelectrics* **1984**, *60*, 3−13.

(19) Mishra, S.; Unnikrishnan, L.; Nayak, S. K.; Mohanty, S. Advances in piezoelectric polymer composites for energy harvesting applications: a systematic review. *Macromol. Mater. Eng.* **2019**, *304*, No. 1800463.

(20) Lallart, M.; Cottinet, P.-J.; Guyomar, D.; Lebrun, L. Electrostrictive polymers for mechanical energy harvesting. *J. Polym. Sci., Part B: Polym. Phys.* **2012**, *50*, 523−535.

(21) Hu, D.; Yao, M.; Fan, Y.; Ma, C.; Fan, M.; Liu, M. Strategies to achieve high performance piezoelectric nanogenerators. *Nano energy* **2019**, *55*, 288−304.

(22) Abbasipour, M.; Khajavi, R.; Akbarzadeh, A. H. A comprehensive review on piezoelectric polymeric and ceramic nanogenerators. *Adv. Eng. Mater.* **2022**, *24*, No. 2101312.

(23) Feng, S.; Zhang, H.; He, D.; Xu, Y.; Zhang, A.; Liu, Y.; Bai, J. Synergistic effects of BaTiO3/MWCNT as fillers on the electrical performance of triboelectric generator based on PDMS composite films. *Energy Technol.* **2019**, *7*, No. 1900101.

(24) Alluri, N. R.; Chandrasekhar, A.; Vivekananthan, V.; Purusothaman, Y.; Selvarajan, S.; Jeong, J. H.; Kim, S.-J. Scavenging biomechanical energy using high-performance, flexible BaTiO3 nanocube/PDMS composite films. *ACS Sustainable Chem. Eng.* **2017**, *5*, 4730−4738.

(25) He, X.; Mu, X.; Wen, Q.; Wen, Z.; Yang, J.; Hu, C.; Shi, H. Flexible and transparent triboelectric nanogenerator based on high performance well-ordered porous PDMS dielectric film. *Nano Research* **2016**, *9*, 3714−3724.

(26) Bouhamed, A.; Jöhrmann, N.; Naifar, S.; Böhm, B.; Hellwig, O.; Wunderle, B.; Kanoun, O. Collaborative filler network for enhancing

the performance of BaTiO3/PDMS flexible piezoelectric polymer composite nanogenerators. *Sensors* **2022**, *22*, 4181.
(27) Mahapatra, B.; Patel, K. K.; Vidya; Patel, P. K. A review on recent advancement in materials for piezoelectric/triboelectric nanogenerators. *Mater. Today: Proc.* **2021**, *46*, 5523−5529.
(28) Tantraviwat, D.; Ngamyingyoud, M.; Sripumkhai, W.; Pattamang, P.; Rujijanagul, G.; Inceesungvorn, B. Tuning the dielectric constant and surface engineering of a BaTiO3/Porous PDMS composite film for enhanced triboelectric nanogenerator output performance. *ACS omega* **2021**, *6*, 29765−29773.
(29) Yun, J. M.; Shin, J. H.; Ryu, J.; Shinde, N. M.; Kim, K. H. Piezoelectric Performance of Cubic-Phase BaTiO3 Nanoparticles Vertically Aligned via Electric Field. *Adv. Sustainable Syst.* **2018**, *2*, No. 1700133.
(30) Anithkumar, M.; Prasanna, A. P. S.; Alluri, N. R.; Kim, S.-J. Self-Powered Smart Touchpad using Novel Intrinsic Piezo−Tribo Hybrid Nanogenerator. *Adv. Funct. Mater.* **2023**, *33*, No. 2213907.
(31) Schädli, G. N.; Büchel, R.; Pratsinis, S. E. Nanogenerator power output: influence of particle size and crystallinity of BaTiO3. *Nanotechnology* **2017**, *28*, 275705.
(32) Sahu, M.; Vivekananthan, V.; Hajra, S.; Khatua, D. K.; Kim, S.-J. Porosity modulated piezo-triboelectric hybridized nanogenerator for sensing small energy impacts. *Applied Materials Today* **2021**, *22*, No. 100900.
(33) Lü, X.; Yu, T.; Meng, F.; Bao, W. Wide-range and high-stability flexible conductive graphene/thermoplastic polyurethane foam for piezoresistive sensor applications. *Adv. Mater. Technol.* **2021**, *6*, No. 2100248.
(34) Chen, C.; Tsai, C.; Xu, M.; Wu, C.; Huang, C.; Lee, T.; Fuh, Y. A fully encapsulated piezoelectric−triboelectric hybrid nanogenerator for energy harvesting from biomechanical and environmental sources. *Express Polym. Lett.* **2019**, *13*, 533−542.
(35) Meisak, D.; Kinka, M.; Plyushch, A.; Macutkevic, J.; Zarkov, A.; Schaefer, S.; Selskis, A.; Samulionis, V.; Kuzhir, P.; Banys, J.; et al. Piezoelectric nanogenerators based on BaTiO3/PDMS composites for high-frequency applications. *ACS omega* **2023**, *8*, 13911−13919.
(36) Manika, G. C.; Andrikopoulos, K. S.; Psarras, G. C. On the ferroelectric to paraelectric structural transition of BaTiO3 micro-/nanoparticles and their epoxy nanocomposites. *Molecules* **2020**, *25*, 2686.
(37) Sahoo, T.; Tripathy, S.; Mohapatra, M.; Anand, S.; Das, R. X-ray diffraction and microstructural studies on hydrothermally synthesized cubic barium titanate from TiO2−Ba (OH) 2−H2O system. *Mater. Lett.* **2007**, *61*, 1323−1327.
(38) Robertson, C.; Roland, C. Glass Transition and Interfacial Segmental Dynamics in Polymer-Particle Composites. *Rubber Chem. Technol.* **2008**, *81*, 506−522.
(39) Plyushch, A.; Macutkevic, J.; Banys, J.; Kuzhir, P.; Kalanda, N.; Petrov, A.; Silvestre, C.; Uimin, M.; Yermakov, A.; Shenderova, O. Carbon-Coated Nickel Nanoparticles: Effect on the Magnetic and Electric Properties of Composite Materials. *Coatings* **2018**, *8*, 165.
(40) Ash, B.; Schadler, L.; Siegel, R. Glass transition behavior of alumina/polymethylmethacrylate nanocomposites. *Mater. Lett.* **2002**, *55*, 83−87.
(41) Arrighi, V.; McEwen, I.; Qian, H.; Prieto, M. B. S. The glass transition and interfacial layer in styrene-butadiene rubber containing silica nanofiller. *Polymer* **2003**, *44*, 6259−6266.
(42) Akbari, B.; Tavandashti, M. P.; Zandrahimi, M. Particle size characterization of nanoparticles−a practical approach. *Iran. J. Mater. Sci. Eng.* **2011**, *8*, 48−56.
(43) Yao, M.; Li, L.; Wang, Y.; Yang, D.; Miao, L.; Wang, H.; Liu, M.; Ren, K.; Fan, H.; Hu, D. Mechanical energy harvesting and specific potential distribution of a flexible piezoelectric nanogenerator based on 2-D BaTiO3-oriented polycrystals. *ACS Sustainable Chem. Eng.* **2022**, *10*, 3276−3287.
(44) Yu, J.; Janolin, P.-E. Defining "giant" electrostriction. *J. Appl. Phys.* **2022**, *131*, 170701.
(45) Moretti, G.; Rosset, S.; Vertechy, R.; Anderson, I.; Fontana, M. A review of dielectric elastomer generator systems. *Adv. Intell. Syst.* **2020**, *2*, No. 2000125.
(46) Jenkins, C. H.; Korde, U. A. Membrane vibration experiments: An historical review and recent results. *Journal of Sound and Vibration* **2006**, *295*, 602−613.
(47) Liu, X.; Zhao, X.; Xie, C. Exact free vibration analysis for membrane assemblies with general classical boundary conditions. *Journal of Sound and Vibration* **2020**, *485*, No. 115484.
(48) Cottinet, P.-J.; Guyomar, D.; Guiffard, B.; Lebrun, L.; Putson, C. Electrostrictive polymer composite for energy harvesters and actuators. *J. Polym. Eng.* **2011**, *31*, 133−140.
(49) Zhang, Q.; Bharti, V.; Zhao, X. Giant electrostriction and relaxor ferroelectric behavior in electron-irradiated poly (vinylidene fluoride-trifluoroethylene) copolymer. *Science* **1998**, *280*, 2101−2104.
(50) Chen, B.; Li, T.; Dong, Q.; Mosconi, E.; Song, J.; Chen, Z.; Deng, Y.; Liu, Y.; Ducharme, S.; Gruverman, A.; et al. Large electrostrictive response in lead halide perovskites. *Nature materials* **2018**, *17*, 1020−1026.
(51) Hoshina, T. Size effect of barium titanate: fine particles and ceramics. *Journal of the ceramic society of Japan* **2013**, *121*, 156−161.

https://doi.org/10.1021/acsaelm.4c01333
ACS Appl. Electron. Mater. 2024, 6, 7464−7474